TRANSIENT 3D SIMULATIONS FOR THE ASTRID REACTOR: PRELIMINARY RESULTS FOR THE ULOF INITIATION PHASE

S. GIANFELICI
Agenzia nazionale per le nuove tecnologie,
l'energia e lo sviluppo economico sostenibile (ENEA)
Bologna, Italy
Email: simone.gianfelici@enea.it

M. MASSONE, A. RINEISKI
Karlsruhe Institute of Technology (KIT)
Karlsruhe, Germany

M. MARCHETTI
Framatome
Paris, France

L. ANDRIOLO, D. LEMASSON, S. POUMEROULY
Electricité de France (EdF)
Paris, France

Abstract

An Unprotected Loss Of Flow transient (ULOF) in the 1500MWth Advanced Sodium Technological Reactor for Industrial Demonstration (ASTRID) reactor is investigated with SIMMER-IV, a 3D multi-phase, multi-velocity and multi-component fluid-dynamics and neutronics code. The 2D RZ code version, SIMMER-III, is a working horse for fast reactor severe accident studies at KIT and other institutions, but the 2D approach affects simulation of reactivity feedbacks and of behavior of reactor materials under accident conditions. On the other hand, 3D SIMMER ULOF calculations take a lot of time and computer memory and were not tried for a full-vessel pool-type fast reactor model at KIT and EdF before recently.

Recent developments for SIMMER-IV, including introductions of a new neutron transport solver based on the PARTISN code and of a new procedure for generation of few-group cross-sections during the transient, offer new simulation capabilities. Also, more computer power is available now. Therefore, an effort was done at KIT, in collaboration with EdF, to perform calculations for a full-vessel 3D model of the primary ASTRID circuit. After a first attempt, modifications were introduced in the code and the employed reactor model for improving their performance.

In the paper we inform on our experience with 3D SIMMER calculations, present preliminary results of 3D steady state and transient simulations for the ULOF initiation phase, do preliminary comparisons with results of 2D analyses.

1. INTRODUCTION

Originally developed for severe accidents analysis in Sodium Fast Reactors (SFRs) [1], the SIMMER code is a flexible tool which has a fluid-dynamic model, capable of simulating multiple phases for the different core materials with different velocity field for the movable components, coupled with a neutronic one, which allows the simulation of reactivity excursions and possible recriticalities due to fuel relocation, as calculated by its structure model. The SIMMER code is currently available for 2D calculations with the SIMMER-III code [2][3][4], and for 3D calculations with the SIMMER-IV code [5][6].

With the increasing availability of computational power, a transition from 2D to full 3D simulations is expected in the near future. The more realistic representation of the reactor core design and its components can lead to a better description of the reactivity effects during transients, especially in the case of core degradation and material relocation [7]. With this in mind, a 3D SIMMER ULOF calculation for the ASTRID reactor has been set up and tested, comparing the results with the data obtained with previous 2D models.

The modelling of a full-vessel pool-type reactor such as the ASTRID (Advanced Sodium Technological Reactor for Industrial Demonstration) design, with both the neutronic and thermal-hydraulic models activated, is, however, still a computational challenging task which requires a high level of parallelization and special considerations to speed up the simulations. For this reason, modifications to the code have been applied and tested.

With these modifications, a 3D SIMMER-IV steady state, followed by an ULOF transient, has been modelled for the Low Void worth Core design version 3 (CVF v3) of the ASTRID reactor.

2. THE ASTRID REACTOR DESIGN

ASTRID (Advanced Sodium Technological Reactor for Industrial Demonstration) is a Gen-IV SFR pool-type reactor of 1500 MWth designed for industrial scale demonstration [8]. Various options have been considered during the design phase to fulfil Gen-IV criteria regarding the safety aspects. The objectives for the so-called CFV (Low Void worth Core) core design [9] include a negative full void coefficient, good fuel burnup performances and intrinsic safety measures during transients. Among them, the design of a core with low total voiding effect aims at the prevention of core degradation and mitigation of a potential severe accident. A summary of the main parameters is reported in Table 1.

The core is subdivided into two zones, inner and outer, with different active region heights and fuel enrichment. All fuel sub-assemblies (SAs) include a sodium plenum zone above the active region, aiming at the reduction of the sodium voiding feedback coefficient. In addition, the inner core subassemblies include an intermediate fertile zone, which limits the power peaking factor and improves the breeding ratio.

Three different types of absorber rods are present in the core: control and shutdown rods (RBC), diverse control and shutdown rods (RBD) and floating safety rods (DCS-P). Additional positions are reserved for core material relocation tubes, which evacuate the molten fissile material from the core in case of a severe accidents, hence limiting the likelihood of a recriticality event and a subsequent power excursion.

Schematics of the vertical and horizontal section of the core layout are shown in Fig. 1.

TABLE 1. CFV CORE PARAMETERS [8][9]

Parameter	Value
Nominal thermal power	1500 MW
Core inlet/outlet temperature	400/550 °C
Mass flow rate through the fuel SAs	7206 kg/s
Inner/outer fissile height	60/90 cm
Inner/lower fertile height	20/30 cm
Inner/outer sodium plenum	40/30 cm
Void reactivity effect, core at equilibrium	-0.5 $ (-184 pcm)

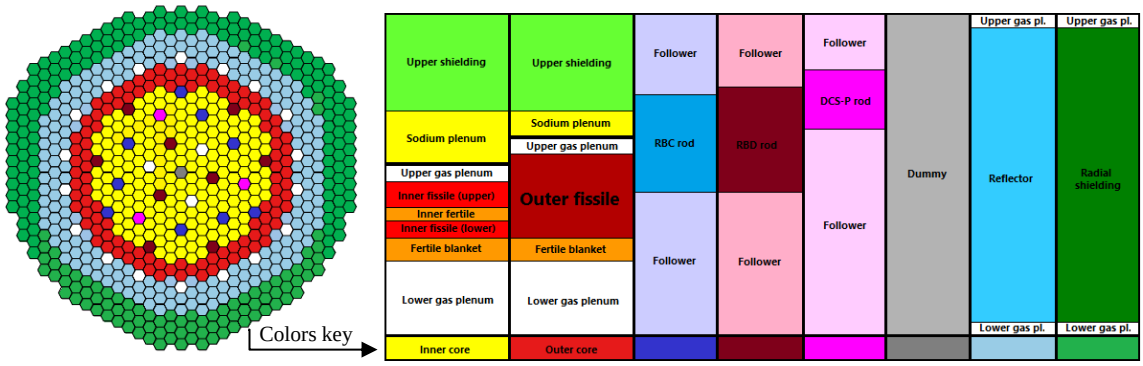

FIG. 1. CFV core, horizontal and vertical sections (based on [8][9])

3. SIMMER MODELS

In 2D SIMMER calculations, the user can model the core in Cartesian (XY) or axial symmetric (RZ) meshes. In the cylindrical symmetry, multiple subassemblies are described by the same ring of the nodalization and the relative position of different subassemblies is approximated using different rings, as shown in Fig. 2; on the contrary, 3D models offer a better description of the reactor core geometry and relative subassemblies position and local effects can be analysed in more detail. In facts, in 3D simulations it is possible to model each single

subassembly; in the employed model each hexagonal SA is represented in plane by a single X mesh and two Y meshes: such subdivision preserves the cross-sectional area and the adjacency between hexagonal SAs, providing an acceptable Cartesian representation of a hexagonal grid. SIMMER still takes into account the hexagonal shape of the SAs through the surface area-to-volume ratio of the hexcan wall.

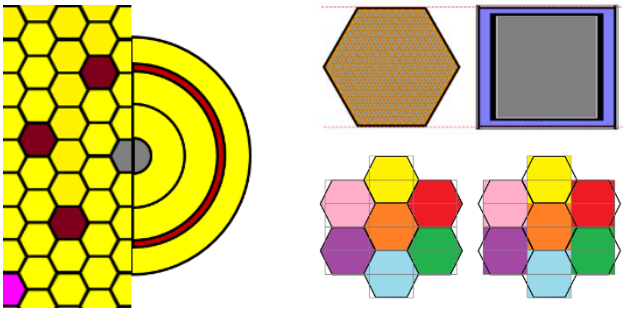

FIG. 2. 2D SAs rings (left) and 3D SAs (right) in SIMMER nodalization

3.1. SIMMER modifications

When modelling a whole reactor core, the use of a fine 3D mesh, with neutronics and thermohydraulic models enabled, is still a very challenging task from a computational standpoint, even in a parallel environment. For this reason, KIT developed computational strategies to accelerate the calculation and limit the iterations needed for each time step.

Several actions are taken regarding the neutronic solver of SIMMER-IV. KIT has developed a correction set [10][11][12] that replaces the original SIMMER transport solver, based on DANTSYS, with the more modern PARTISN [13], which features parallelization capabilities; parallelization has been introduced also in the cross-section generation and self-shielding procedure. In addition, a multi-group cross-section collapsing technique [14][15] is implemented to condense at every time step, with approximately computed cell-dependent neutron flux spectra, the 11-groups cross-sections library usually used at KIT for SFR calculations [16][17], into a 4-groups ones. In addition, a special modelling for the inter-SA sodium, located in no-flow-zones between the SAs, is adopted, so that these zones are filled with sodium rather than voided from the neutronics point of view.

During the progression of the calculations, it has been noticed that a slow flux convergence is achieved when cells with very low flux values are included in the convergence iteration. In these cells the absolute values of the flux are low, but the actual variation may be significant in relative terms. For this reason, the neutron flux convergence criteria have been eased at the point-wise level.

3.2. 2D nodalization

The original SIMMER-III calculation was performed with an axial-symmetric 2D model, featuring 44 radial subdivisions and 93 axial ones, as shown in Fig. 3. The pumps are simulated with the corresponding SIMMER model; the intermediate heat exchangers (IHXs) are emulated using a section of steel rods set at the sodium inlet temperature in the core (400 °C) and with a very large density in order to accommodate the heat transferred from the sodium. The core region is composed of 18 SA rings, of which 11 dedicated to fuel rods and the others to control and safety rods. Inner and outer fuel SAs have different heights as shown in Fig. 3; the sodium plenum is visible between the fuel rod and the upper shielding.

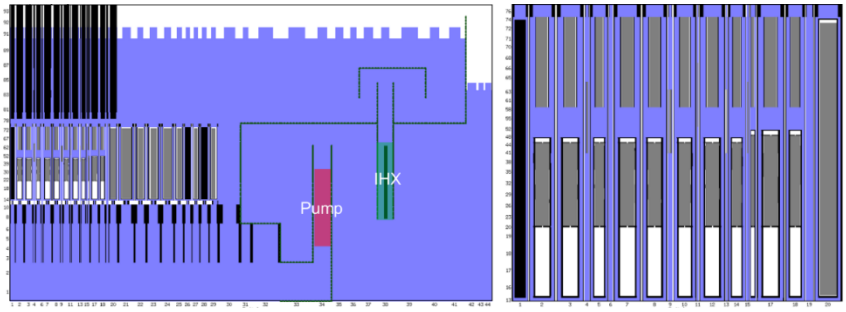

FIG. 3. SIMMER-III 2D nodalization: vertical section of the SIMMER model (left) and detail of the CFV core (right)

3.3. 3D nodalization

Horizontal and vertical sections of the SIMMER-IV model, together with a picture of the coolant path and the main reactor components, are shown in Fig. 4. The fluid-dynamics mesh is composed by 27×54×76 cells in XYZ geometry, each hexagonal subassembly being represented in plane by a single X mesh and two Y meshes. Exclusively the core and the reflector are modelled, while the radial shield is excluded to reduce the number of meshes involved, considering its limited effect on both neutronics and thermal-hydraulics of the reactor system. The available out-of-core cells in the corners are employed to specify four channels (in green and red in Fig. 4, center) required for the whole vessel modelling, two for the pumps and two for the heat exchangers; using the corner limits the number of meshes required for the whole vessel model, so reducing the required computational resources.

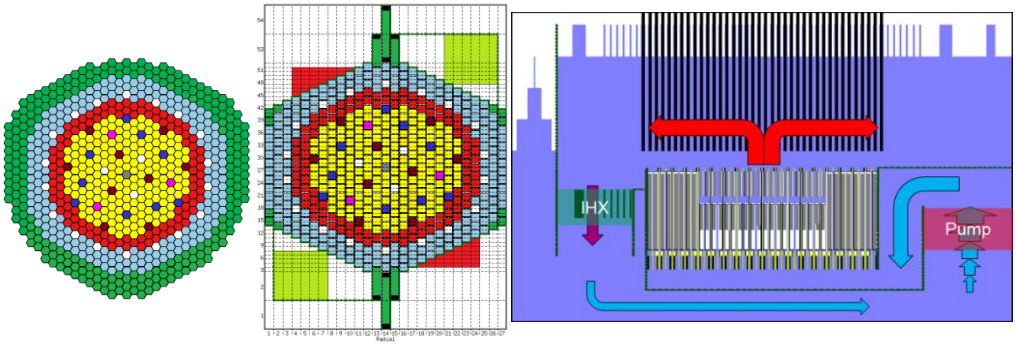

FIG. 4. SIMMER IV nodalization: comparison between the horizontal sections of the CFV core (left) with the SIMMER model (center); SIMMER model axial section with flow path (right). Pumps in red, IHXs in green.

4. RESULTS

The calculation is performed in two main steps. The focus of the first step is the establishment of steady state conditions at fixed design power and the tuning of the model for temperatures and flow rates. During this first calculation, the reactivity of the system is assessed. In the second step, together with the ULOF data, the user can then input an external reactivity to compensate the calculated one and start the transient calculation with a critical reactor.

4.1. Steady state calculation

In this first step, a calculation at fixed power is performed to evaluate the structures and fluids temperatures and establish the flow rate of the coolant; the main quantities evaluated at the end of this process are reported in Table 2. Linear Heat Rates (LHRs) have also been checked in different positions of the reactor core: for the innermost SA of the inner core; for the outermost one; for the outer core. As it can be noticed in Fig. 5, the effect of the inner fertile layer is visible in the middle section of the inner core subassemblies, while the outer core does not have any intermediate layer.

TABLE 2. SIMMER STEADY STATE PARAMETER

Parameter	Value
Nominal thermal power	1501 MW
Averaged Core inlet/outlet temperature	400/561 °C
Mass flow rate through the fuel SAs	7240 kg/s

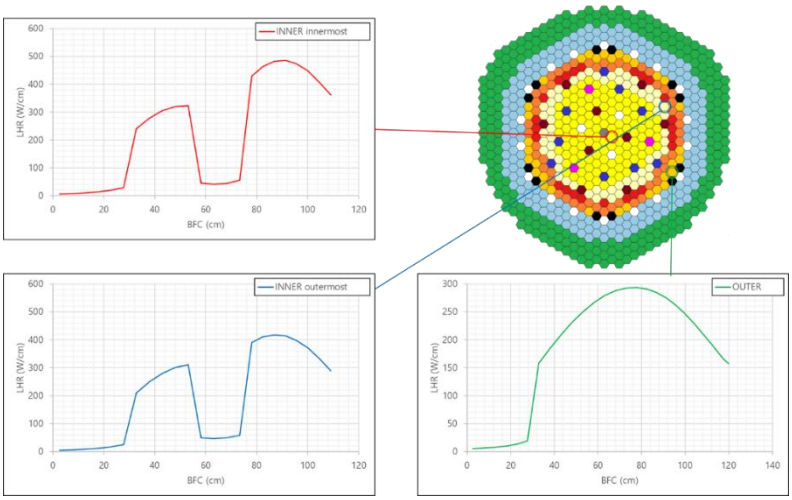

FIG. 5. SIMMER-IV Axial power profiles for different core positions

Fig. 6 shows the reactivity trend of the fixed power calculation (to be compensated in the next calculation step). After 150 s of simulation, the final value of the global reactivity is -0.627 $. This value has been used as an input for the ULOF transient calculation with free power.

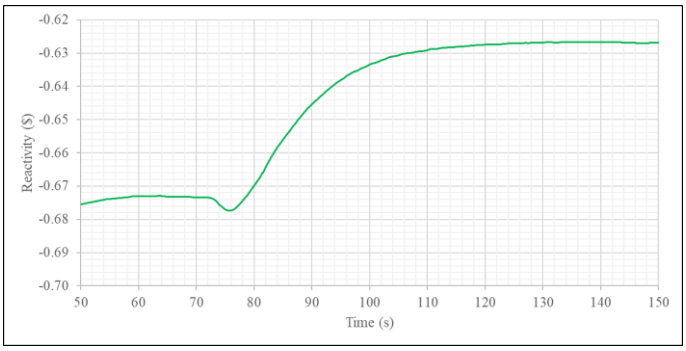

FIG. 6. SIMMER global reactivity during the steady state calculation

The radial temperature profile within the fuel is discretized with two nodes, an inner bulk node and a surface node; the thickness of the surface node corresponds to the thermal penetration depth, as evaluated by the code. Special attention has been put on the SIMMER fuel temperatures, reported in Table 3, in the inner and outer core, checking that they lie in a reasonable range. Three core sections have been considered: the upper fissile zone of the inner core; the lower fissile zone of the inner core; the fissile zone of the outer core. The maximum values of bulk and surface temperatures occur in the upper fissile zone of the inner core, with a bulk temperature of 2263 °C and a surface temperature of 914 °C; for the outer core the bulk temperature reaches 2029 °C and the surface temperature 851 °C. The maximum fuel temperatures are observed at the interface between the inner and the outer core, since the core has a Beginning Of Life (BOL) composition.

TABLE 3. SIMMER FUEL TEMPERATURES

Zone	Max fuel bulk T (°C)	Min fuel bulk T (°C)	Max fuel surface T (°C)	Min fuel surface T (°C)	Mass Av. Fuel T (°C)
Inner (upper fissile)	2263	1605	915	761	2034
Inner (lower fissile)	1865	1247	746	575	1624
Outer	2029	930	851	518	1500

4.1.1. Neutronic parameters

The void feedback coefficients of the developed model have been calculated with SIMMER and compared with a 3D ERANOS [18] model, which is considered the neutronic reference. ERANOS employs 33-groups cross-section libraries, pre-processed using the cell code ECCO starting from fine structure libraries with 1968 groups [19]; P3 approximation is used.

The comparison results, reported in Table 4, show that SIMMER with its 11-groups libraries correctly estimate the plenum void feedback coefficient, but overestimates the core one. This leads to an overestimation of the full void coefficient, which is anyhow negative, as predicted by ERANOS. The cross-section condensation procedure, from 11 to 4 groups, has indeed a relatively small impact on the feedback coefficients, as shown in [14], slightly in the direction of the ERANOS results. The group structure of the employed libraries are shown in Table 5.

Hence, it is considered justified the use of the 11-groups libraries collapsed to 4 groups, also in consideration that a 3D calculation performed with a larger number of groups would further increase the required computational resources, which are already high.

TABLE 4. VOID REACTIVITY COEFFICIENTS EVALUATION

Model	Groups / XS collapsing	Void Plenum (pcm)	Void Core (pcm)	Void Full (pcm)
SIMMER	11 g	-1254	+1209	-247
SIMMER with XS collapsing	11→ 4 g	-1290	+1157	-349
ERANOS (P_3)	33 g	-1342	+995	-608

TABLE 5. CROSS-SECTION LIBRARY GROUP STRUCTURE

11 groups						
	1.05E+7 eV	6.50E+6 eV	2.50E+6 eV	8.00E+5 eV	2.00E+5 eV	1.00E+5 eV
	4.65E+4 eV	1.00E+4 eV	2.15E+3 eV	1.00E+3 eV	1.00E+2 eV	1.00E-5 eV
4 groups						
	1.05E+7 eV	8.00E+5 eV	4.65E+4 eV	1.00E+3 eV	1.00E-5 eV	

4.2. ULOF calculation

Both 2D and 3D calculations start from a developed steady state with balanced reactivity and share the same assumptions: in an Unprotected Loss Of Flow, control and shutdown rods are not inserted in the core during the transient; in our calculations, also the movement of the floating safety rods DCS-P, supposed to move with the decreasing flow rate, is not considered.

Different evolutions of the transient have been observed in the two models: the 2D calculation ran for 67.15 s from ULOF start, stopping for convergence issues after a relevant power insertion; meanwhile, even considering the considerable amount of time required, the 3D calculation is still ongoing after 72.5 s from ULOF start.

4.2.1. Pump coast down

The pump coast down curve used for the transient simulation considers a pump halving time of 10 s and a full stop of the flow at 107 s, as shown in Fig. 7. Since SIMMER allows to specify the driving pressure for the implemented pump model, a quadratic correlation of the flow rate trend is adopted for evaluating the needed driving pressure curve.

Due to the approximation of the input pressure curve, the flow rate evaluated by SIMMER is slightly lower than expected and in agreement between the codes. This underestimation could be fixed by adjusting the pressure curve in several iterations, but this would need a large amount of additional time for the iterative procedure. Nonetheless, the trend of the flow rate is very close to the desired trend and can be considered acceptable for most

purposes. A partial reduction between the reference and SIMMER flow rates can be noticed after 30 s, probably due to the contribution of the natural circulation in the full vessel model.

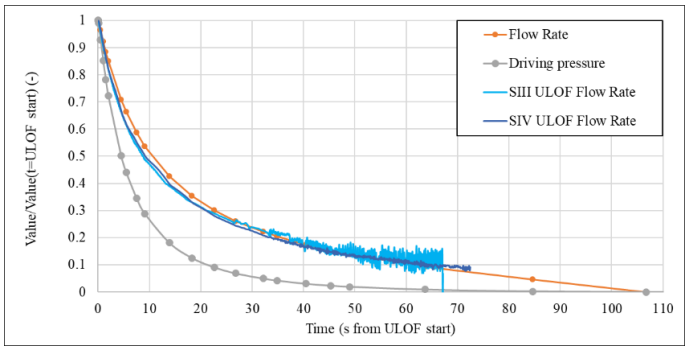

FIG. 7. Pump coast down and driving pressure curves

4.2.2. Core power and reactivity

The normalized power trends for both codes show an initial decrease to around 80% of the nominal value in the first 20 s of the ULOF transient. After this point, a significant sodium boiling event starts and the evolution of the two calculations diverge significantly. The sodium boiling and rewetting behavior in the inner core sodium plenum leads to reactivity oscillations as shown in the right graph of Fig. 8.

In the case of 3D, the oscillations are milder, with the reactivity constantly remaining below zero, leading to a continuous decrease of the power levels. Conversely, in 2D geometry the reactivity swings are much wider, reaching values above zero and so leading wider power swings.

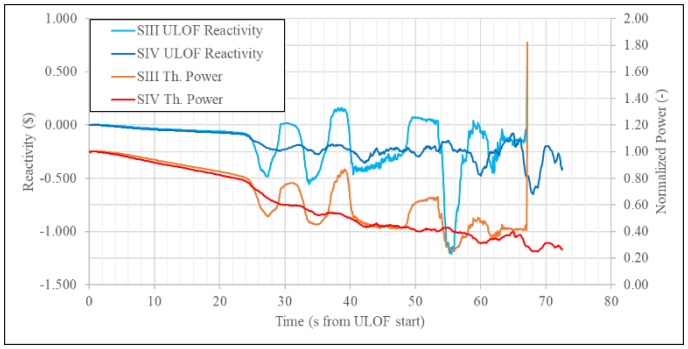

FIG. 8. ULOF transient reactivity vs. power history

Since the reactivity and power trends described in the previous section are heavily influenced by the sodium boiling and rewetting in the various sections of the core, in order to better understand the reasons behind the boiling effects on the reactivity, quantities for the sodium plenum area and for the fuel columns have been computed separately. The volume of the vapor in these zones has been then integrated and compared to the trend of the reactivity and the volume of the vapor in the core during the transient. This evaluation was performed for 2D and 3D and the comparisons and the integration volumes are shown in Fig. 9.

An early formation of vapor in the sodium plenum is calculated by SIMMER for both codes. This appears to have a limited effect on the reactivity until the vapor volume in the plenum reaches a value of about 0.01 m3 at 24 s, when a steep increase in vapor formation in the zones with the highest power leads to a first reactivity swing. The amount of vapor initially present in the sodium plenum is higher for the 2D case. 3D models are in general characterized by lower coolant void/density effects due to a higher neutron leakage in 3D. It should also be noticed that the usually larger numbers of meshes as compared to 2D ones can simulate coolant voiding onset in more detail and in smaller regions because of their larger number and smaller volumes. Alternatively or in addition, sodium boiling may occur later because of this combination of effects. Voiding/condensation evolution is then more gradual and the reactivity swings are to be less pronounced compared to 2D ones during the initiation phase. This may lead to simulation results showing a milder transient evolution in the 3D case, with postponed or avoided

massive core melting. This can be noticed already at the beginning of the sodium boiling, with higher reactivity and power swings in the 2D case. The higher energy deposition leads to higher sodium vapor production and exacerbate the vaporization/condensation process, affecting the power history during the transient.

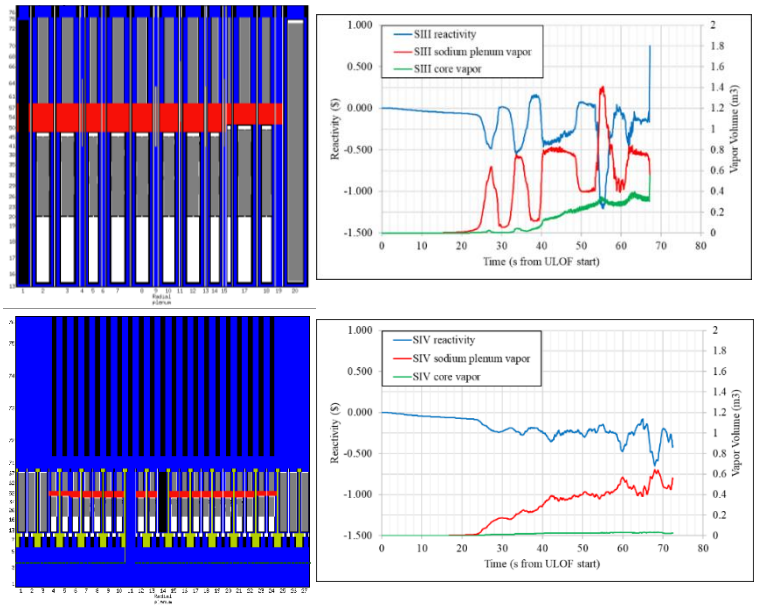

FIG. 9. 2D SIMMER-III (above) and 3D SIMMER-IV (below):
Sodium plenum zone in red (left), reactivity history compared to the vapor volume fraction in the core and sodium plenum (right)

4.2.3. Pin and SA failures

In the 3D calculation SIMMER predicts the first pin failure 39.3 s after ULOF start; after 64.3 the first can wall failure is detected. After 72.5 s, the last considered time in the 3D calculation, 8 subassemblies in the outer core zone show pin failures, of which 2 with can wall failures. These failures are located in the SA of the outer core, where the power is higher due to Beginning Of Life (BOL) core configuration. However, no fuel melting is observed.

An interesting behavior was observed for the 2D calculation, especially at the end of the transient. The first pin failure is detected in the first ring (out of 3) of the outer core at 44.15 s, with the channel completely voided in the active zone. The third ring shows a similar behavior, with pin failure at 59.9 s. Molten material erodes the hexcan wall of the first ring, which fails on the left side at 62.1s. The pictures of the final stages of the calculation are shown in Fig. 10. At 67.1 s from ULOF start (60 s) the wall fails on the right side. The sodium vapor enters the second outer core ring, increasing the sodium vapor volume in the active zone and pushing the liquid sodium in the sodium plenum. These concurrent events increase the reactivity up to 0.75 $ and a final power peak is calculated. Thus the final power peak is not caused by an increase in sodium boiling, but by a can wall failure and a vapor insertion in a channel still filled with liquid sodium.

Comparing the 2D and 3D discretizations, an event such as a can wall failure involves all of the SAs discretized in one ring of the bidimensional model, instead of a limited number of SAs in the 3D model. In this case, the insertion of sodium vapor in the active core zone from one mesh to the other has a much stronger impact on the reactivity feedbacks and on the global reactivity, leading to the final power insertion at the end of the evaluated transient time.

It should be noticed that, in order to limit the computational time for the 3D case, the calculations have been performed with the so called “simplified pin” model implemented in SIMMER. More reliable pin failure behavior simulation can be obtained using the SIMMER “detailed pin” model, possibly coupled with external fuel performance codes [20]. Nonetheless, the presented results are considered comparable since the same model has been used for both 2D and 3D cases.

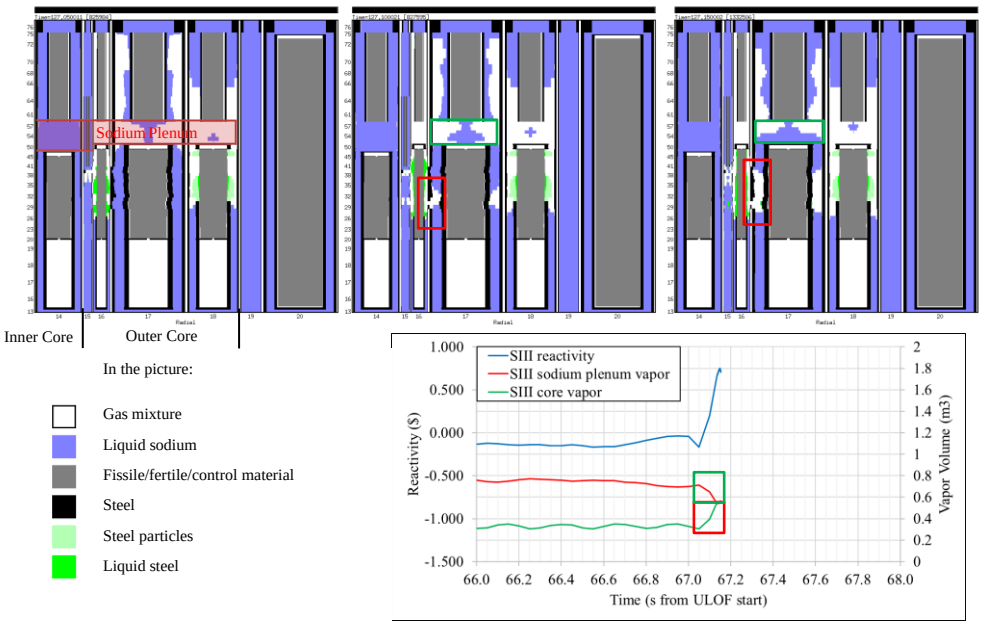

FIG. 10. SIMMER-III calculation, final power excursion

5. CONCLUSIONS

With the availability of new computational machines and techniques, a 3D model calculation has been set up and used as basis for a steady state and a ULOF transient analyses for the ASTRID reactor. The results obtained have been compared to previous 2D calculations to assess the possible effects of the different representations on the evolution of the transient.

Due to the computational power required, modifications to the code have been applied with the aim of speeding up the calculation; in addition, special attention has been put in limiting the core and vessel model size. Nonetheless, the computation of such a case is still very challenging with the current SIMMER version, despite KIT optimizations of its neutronics part with PARTISN: the simulation of about 72.5 s of ULOF transient, steady state included, has taken almost one year of computation. Further improvement in performance can be achieved with a greater degree of parallelization, which is a key feature in the new SIMMER-V code [21].

Nonetheless, the preliminary results show interesting differences over the 2D counterpart, especially regarding the sodium boiling and rewetting behavior, which greatly affects the reactivity swing and thus the power evolution during the ULOF transient. The 2D model shows wider initial power and reactivity swings, leading to higher amount of sodium vapor in the active core zone and affecting the final stages of the transient. On the contrary, the 3D model estimates a limited amount of vapor in the active core zone and, even if the boiling and rewetting of the sodium plenum causes reactivity and power oscillation, the reactivity remains below zero for the simulation time reported. This effect is probably related to the more precise geometric description given by the 3D representation: while in 3D pin failure is observed before than in 2D, the effect remains localized to a few cells rather than affecting a whole fuel ring. This results in more accurate feedback coefficient assessment and milder transients.

The results demonstrate the applicability of SIMMER-IV to full vessel SFRs for the simulation of ULOF initiation phase. This applicability was up to now restricted by the very high computation costs and very long simulation times, and full vessel SFR models for transient analyses at KIT were mainly performed with the 2D SIMMER-III code. These limitations have been eased recently. An implementation of the SIMMER-PARTISN coupling at KIT brings to SIMMER a new highly parallelized neutron transport solver. The high performance of this solver is improved by employing a new SIMMER correction set that reduces the number of energy groups used in PARTISN, while preserving the neutron balance. In addition, the convergence checking in PARTISN is optimized and effectively excludes from consideration the cells in remote regions of the 3D model with very small neutron fluxes. Availability of a new computer cluster for parallel calculations at KIT made possible parallel calculations in both neutronics and fluid-dynamics parts of the code. The established model and code versions offer a basis for further SIMMER-IV code and 3D ASTRID model optimizations. They may help to accelerate

3D calculations further, thus opening ways for routine application of 3D models for the initiation phase and for investigation of SIMMER-IV applicability to 3D simulations of later phases of ULOF, such as transition to full core melting and mechanical energy release under hypothetical accident conditions.

ACKNOWLEDGEMENTS

The authors acknowledge support by the state of Baden-Württemberg through bwHPC.

REFERENCES

[1] BOHL, W.R., LUCK, L.B., SIMMER-II: A Computer Program for LMFBR Disrupted Core Analysis, LA-11415-MS, Los Alamos National Laboratory, Los Alamos, 1990.
[2] KONDO, S., YAMANO, H., SUZUKI, T. et al., SIMMER-III: A Computer Program for LMFR Core Disruptive Accident Analysis, Version 2.H Model Summary and Program Description, TN9400 2001-2002, Japan Nuclear Cycle Development Institute, 2000.
[3] TOBITA, Y., KONDO, S., YAMANO, H. et al., "The Development of SIMMER-III, An Advanced Computer Program for LMFR Safety Analysis", Use of Computational Fluid Dynamics (CFD) Codes for Safety Analysis of Reactor Systems Including Containment, (Proc. of the IAEA/NEA Technical Meeting, Pisa, 2002), IAEA (2002).
[4] YAMANO, H., FUJITA, S., TOBITA, Y. et al., SIMMER-III: A Computer Program for LMFR Core Disruptive Accident Analysis, TN9400 2003-071, Japan Nuclear Cycle Development Institute, 2003.
[5] KONDO, S., YAMANO, H., TOBITA, Y. et al., SIMMER-IV: A Three-Dimensional Computer Program for LMFR Core Disruptive Accident Analysis, Japan Nuclear Cycle Development Institute, JNCTN9400 (2000).
[6] YAMANO, H., FUJITA, S., TOBITA, Y. et al., Development of a three-dimensional CDA analysis code: SIMMER-IV and its first application to reactor case, Nuc. Eng. Des. **238** 1 (2008), 66–73.
[7] BERTRAND, F. et al., Mitigation of severe accidents for SFR and associated event sequence assessment, Nuc. Eng. Des. **372** (2021).
[8] ROUAULT, J., et al., "ASTRID, the SFR GEN IV technology demonstrator project: where are we, where do we stand for?", Advances in Nuclear Power Plant ICAPP 2015 (Proc. Int. Cong., Nice, 2015), ANS (2015).
[9] BECK, T., et al., Conceptual design of ASTRID fuel sub-assemblies, Nuc. Eng. Des. **315** (2017) 51-60.
[10] MARCHETTI, M., et al., "The SIMMER/PARTISN Capability for Transient Analysis", The Role of Reactor Physics toward a Sustainable Future PHYSOR 2014 (Proc. Int. Conf., Kyoto, 2014), ANS (2014).
[11] VEZZONI, B., MARCHETTI, M., ANDRIOLO, L. et al., "SIMMER/PARTISN analyses of EBR-II shutdown heat removal tests", Physics of Reactors 2016 PHYSOR 2016 (Proc. Int. Conf., Sun Valley, 2016) ANS (2016).
[12] VEZZONI, B. et al., "IAEA EBR-II neutronics benchmark: Impact of modeling options on KIT results", Physics of Reactors 2016 PHYSOR 2016 (Proc. Int. Conf., Sun Valley, 2016) ANS (2016).
[13] ALCOUFFE, R.E., BAKER, R.S., PARTISN: A Time-Dependent, Parallel Neutral Particle Transport Code System. LA-UR-08-07258, Los Alamos National Laboratory, Los Alamos, 2008.
[14] MASSONE, M., GABRIELLI, F., RINEISKI, A., SIMMER extension for multigroup energy structure search using genetic algorithm with different fitness functions, Nuc. Eng. Tech. **49** 6 (2017) 1250-1258.
[15] MASSONE, M., Cross-sections for transient analyses: development of a genetic algorithm for the energy meshing, Ph.D. Thesis, Karlsruhe (2018).
[16] RINEISKI, A., SINITSA, V., GABRIELLI, F., MASCHEK, W., "C4P Cross-section Libraries for Safety Analyses with SIMMER and related studies", Mathematics and Computational Methods Applied to Nuclear Science and Engineering MC 2011 (Proc. Int. Conf., Rio de Janeiro, 2011), ANS (2011).
[17] KIEFHABER, E., Updating of an 11-groups nuclear cross section set for transmutation applications, Mu hl, B. (Ed.), Projekt Nukleare Sicherheitsfoschung, Jahresbericht 1999, FZKA-6480, Karlsruhe, 2000.
[18] RIMPAULT, G., PLISSON, D., TOMMASI, J. et al., "The ERANOS code and data system for fast reactor neutronic analyses", New Frontiers of Nuclear Technology: reactor physics, safety and high-performance computing PHYSOR 2002 (Proc. Int. Conf., Seoul, 2002), ANS (2002).
[19] RIMPAULT, G., "Algorithmic features of the ECCO Cell Code for treating heterogeneous fast reactor subassemblies", Mathematics and computations, reactor physics, and environmental analyses (Proc. Int. Conf., Portland, 1995), ANS (1995).
[20] GIANFELICI, S., et al., Validation of the FEMAXI/SIMMER coupling by using the E9 CABRI-2 experiment, EPJ Web Conf. **247** (2021).
[21] BACHRATA, A. et al., Severe accident studies on the efficiency of mitigation devices in a SFR core with SIMMER code, Nuc. Eng. Des. **373** (2021).